An acetylcholine receptor lacking both γ and ε subunits mediates transmission in zebrafish slow muscle synapses

Rebecca Mongeon,[1,2] Michael Walogorsky,[1] Jason Urban,[3] Gail Mandel,[1,2] Fumihito Ono,[3] and Paul Brehm[1]

[1]Vollum Institute and [2]Howard Hughes Medical Institute, Oregon Health and Science University, Portland, OR 97239
[3]National Institute on Alcohol Abuse and Alcoholism, National Institutes of Health, Rockville, MD 20852

Fast and slow skeletal muscle types in larval zebrafish can be distinguished by a fivefold difference in the time course of their synaptic decay. Single-channel recordings indicate that this difference is conferred through kinetically distinct nicotinic acetylcholine receptor (AChR) isoforms. The underlying basis for this distinction was explored by cloning zebrafish muscle AChR subunit cDNAs and expressing them in *Xenopus laevis* oocytes. Measurements of single-channel conductance and mean open burst duration assigned $\alpha_2\beta\delta\varepsilon$ to fast muscle synaptic current. Contrary to expectations, receptors composed of only αβδ subunits (presumed to be $\alpha_2\beta\delta_2$ receptors) recapitulated the kinetics and conductance of slow muscle single-channel currents. Additional evidence in support of γ/ε-less receptors as mediators of slow muscle synapses was reflected in the inward current rectification of heterologously expressed $\alpha_2\beta\delta_2$ receptors, a property normally associated with neuronal-type nicotinic receptors. Similar rectification was reflected in both single-channel and synaptic currents in slow muscle, distinguishing them from fast muscle. The final evidence for $\alpha_2\beta\delta_2$ receptors in slow muscle was provided by our ability to convert fast muscle synaptic currents to those of slow muscle by knocking down ε subunit expression in vivo. Thus, for the first time, muscle synaptic function can be ascribed to a receptor isoform that is composed of only three different subunits. The unique functional features offered by the $\alpha_2\beta\delta_2$ receptor likely play a central role in mediating the persistent contractions characteristic to this muscle type.

INTRODUCTION

Skeletal muscle fiber types are distinguished formally on the basis of contractility (Gilly and Hui, 1980), but many of the biophysical properties relating to ion channels are also quite distinct. For example, in contrast to fast twitch muscle, both slow twitch and tonic muscle types are generally inexcitable and rely on synaptic depolarization to generate contractions (Hidaka and Toida, 1969; Stefani and Steinbach, 1969; Bondi et al., 1986). This distinction also applies to the fast and slow muscle types comprising the tail skeletal muscle of zebrafish (Buckingham and Ali, 2004). Additionally, the synaptic currents recorded from slow muscle types have revealed consistently slower kinetics than the fast muscle counterparts in mammals, frogs, snakes, and fish (Dionne and Parsons, 1978, 1981; Miledi and Uchitel, 1981; Fedorov et al., 1982; Uchitel and Miledi, 1987; Henderson and Brehm, 1989; Ruff and Spiegel, 1990; Luna and Brehm, 2006). Both noise analysis estimates (Dionne and Parsons, 1978; Uchitel and Miledi, 1987) and single-channel measurements of acetylcholine (ACh)-activated receptors (Dionne and Parsons, 1981; Henderson and Brehm, 1989; Ruff and Spiegel, 1990) point to the existence of functionally distinct nicotinic receptor isoforms as causal to the differences in synaptic kinetics. In no case, however, have the bases for these functional distinctions between slow and fast muscle currents been established. One attractive idea derives from the original studies of neuromuscular synapse development in *Xenopus laevis* (Kullberg et al., 1977, 1980, 1981; Brehm et al., 1984) and rat (Sakmann and Brenner, 1978; Fischbach and Schuetze, 1980). In these preparations, at early times in development, the synaptic currents undergo a conversion from slow to fast decay kinetics. The conversion, once thought to result from posttranslational modification (Michler and Sakmann, 1980), was subsequently shown to result from a switch from γ- to ε-containing receptors (Mishina et al., 1986). The idea that the prolonged synaptic decay in slow muscle results from retention of γ subunit–containing receptors received some support from studies on frog pyriformis (Henderson and Brehm, 1989) and snake muscle (Dionne, 1989; Ruff and Spiegel, 1990), where two channel classes were recorded bearing the hallmark conductance differences between ε- and γ-containing channels. In both cases, the lower conductance channel exhibited longer burst durations often associated with γ-subunit receptors. In frog, however, the kinetics did not match the slow synaptic current

Correspondence to Paul Brehm: brehmp@ohsu.edu
Abbreviations used in this paper: ACh, acetylcholine; AChR, ACh receptor.

The Rockefeller University Press $30.00
J. Gen. Physiol. Vol. 138 No. 3 353–366
www.jgp.org/cgi/doi/10.1085/jgp.201110649

kinetics well. Thus, it has remained an open question as to whether ε and γ receptors could fully account for the differences in fast and slow muscle function.

Single-channel recordings from zebrafish muscle challenged the idea that synaptic kinetics of slow muscle were conferred by γ-containing ACh receptors (AChRs). Although cell-attached recordings revealed two amplitude classes with a conductance ratio consistent with ε and γ receptors, the mean open times were indistinguishable (Nguyen et al., 1999). In this study, we compare the kinetics of heterologously expressed zebrafish AChR isoforms to the native receptors in either slow or fast muscle. Although exogenous ε-containing receptors fully matched endogenous fast muscle synaptic currents, neither γ- nor ε-containing receptors could account for the slow decay of synaptic current in slow muscle. Rather, our recordings support the proposal that an AChR isoform lacking both γ and ε subunits underlies the slow synaptic current in zebrafish. Consistent with this idea, expression of both mouse and bovine αβδ receptor subunits gives rise to functional channels in heterologous cells (Jackson et al., 1990; Charnet et al., 1992; Liu and Brehm, 1993), but a bona fide physiological role of αβδ in muscle has never been identified before this study.

MATERIALS AND METHODS

Cloning and expression of zebrafish AChR subunits

Full-length sequences of AChR subunits α and δ were amplified with primers derived from published sequences (Sepich et al., 1998; Ono et al., 2004). Full-length sequences of β1a, β1b, γ, and ε were predicted from the genomic database (National Center for Biotechnology Information) and amplified from cDNA of wild-type zebrafish larvae. GenBank/EMBL/DDBJ accession numbers for each sequence are as follows: β1a (JN242068), β1b (JN242069), γ (JN242070), and ε (JN242071). The obtained cDNA of each subunit was cloned into the pTNT vector (Promega) for in vitro transcription. The purified DNA plasmid was linearized at the BamHI site and in vitro transcribed with T7 RNA polymerase (mMessage mMachine kit; Invitrogen). RNA stocks were produced at 1 μg/μl concentrations.

Zebrafish animal care and strains

Zebrafish (*Danio rerio*) were maintained in accordance with the standards set forth by the International Animal Care and Use Committee. The acetylcholinesterase mutant strain *zim*^{tm205} was obtained from G. Downes (University of Massachusetts, Amherst, MA). Commercially available wild-type zebrafish (Brian's strain) were obtained from J. Fetcho (Cornell University, Ithaca, NY).

Zebrafish neuromuscular synaptic recordings

Zebrafish larvae between 72 and 85 hpf were anesthetized and decapitated before removal of the topside of skin along the entire tail (Wen and Brehm, 2010). Unless otherwise noted, all chemicals were obtained from Sigma-Aldrich. Exposed tail musculature was treated with 10% formamide (vol/vol) in muscle bath solution (in mM: 130 NaCl, 10 Na-HEPES, 3 KCl, 2 $CaCl_2$, and 1 $MgCl_2$; 276 mOsm, pH 7.4) for 2 min, followed by five rinses with bath solution to inhibit contraction. For slow muscle synaptic currents, only the overlying skin was removed, whereas recordings from fast muscle required removal of the slow muscle layer. Slow muscle cells were removed individually using a large bore pipette (15–30 μm) under gentle suction (Wen and Brehm, 2010). Fast and slow muscle spontaneous synaptic currents were recorded in the whole cell voltage-clamp configuration using an amplifier (EPC-10/2; HEKA). Recording electrodes were pulled to an outer diameter of ∼3 μm, lightly fire-polished, and filled with muscle internal solution containing (in mM) 120 KCl, 10 K-HEPES, and 5 K-BAPTA, resulting in electrode resistances between 2 and 3.5 Mohms. Spontaneous synaptic events were sampled at 100 KHz at a −90-mV holding potential. Individual events were detected offline, and the decay phase (10–90%) was fit with either single- or biexponential curves using MiniAnalysis software (Synaptosoft, Inc.). Rising phases of synaptic currents were not fit because of the distortion arising from the frequency limitations of the electronics.

Xenopus oocyte macroscopic recordings

Manually defolliculated stage V *Xenopus* oocytes were injected with 36 ng of synthetic RNA for each AChR subunit. Oocytes were maintained in OR-3 media (Liu and Brehm, 1993) and used for recordings within 1 to 5 d after injection. Whole oocyte current responses to applied ACh were recorded using a two-microelectrode voltage clamp (TEV 200; Dagan Corporation). Oocytes were held at −80 mV and perfused with either a bath solution (in mM: 130 NaCl, 10 Na-HEPES, 3 KCl, 0.2 $CaCl_2$, and 1 $MgCl_2$) or bath solution containing 30 μM ACh at a rate of ∼5 ml/min. Three consecutive trials of ACh application were used to determine the average maximal current response per oocyte. For current–voltage measurements using macroscopic currents, oocytes were injected with 50 nL of 100 mM BAPTA ∼10 min before recording to reduce possible contaminant calcium–activated currents (Haghighi and Cooper, 2000; Nishino et al., 2011).

Single-channel recordings

Combinations of AChR subunit RNAs that resulted in >1-μA peak macroscopic current (in response to 30 μM ACh at −80 mV) were further tested using outside-out patch single-channel recordings. Treatment of the oocyte with 1× trypsin EDTA in bath solution loosened the vitelline membrane for mechanical removal. Recording electrodes with an outer tip diameter of ∼3 μm were coated with elastomer (Sylgard; Dow Corning) and lightly fire-polished. The electrodes were filled with a solution containing (in mM) 80 KF, 20 KCl, 10 K-HEPES, 10 K-EGTA, and 1 $MgCl_2$. Flowing a bath solution containing 300 nM ACh onto the outside-out patch activated the AChR channels. On-muscle cell-attached recordings of ACh-activated single channels were performed with similar electrodes but were filled with muscle bath solution containing added ACh (300 nM). Single-channel currents were recorded using an amplifier (Axopatch 200B; Molecular Devices) and sampled at 100 kHz.

For analysis, single-channel records were digitally filtered offline at 5 kHz, and individual channel events were detected based on half-amplitude tracking. TAC software (Bruxton Corporation) was used to measure the open time, amplitude, and closed gap intervals for each sequential event. Overlapping events were not analyzed, and patches with significant event overlap were not analyzed. Events briefer than 200 μsec in duration were discarded, as we were able to fully resolve the amplitude of openings of longer duration. Closed and open burst-duration histograms were fitted to transformed exponential functions (Sigworth and Sine, 1987), and the amplitude distribution was fit to either single or multiple Gaussian functions using TACfit (Bruxton Corporation).

Data analysis

Data were fit as indicated using IGOR software (WaveMetrics), and statistical significance was determined by pairwise comparisons using Student's *t* test.

Morpholinos

Antisense morpholino oligonucleotides (MOs) were designed to either the translation start site or a splice site for α, γ, and ε mRNA transcripts according to the manufacturer's suggestions (Gene Tools, LLC). The MO sequences were as follows: α, TTCATTTCTGTTGATATGACTGGA; γ, CATGGTTGAAATCCTGA-GAGAAACA; γ_2, TGGTTGAAGGCTCTCCAGTACCTAGT; γ_{SPLICE}, TAATTAA-GGCACATACTCACTTCCC; ε, TGCCGAATCTCTCGGCCACGGCCAT. 0.5–1.5 nL of individual MOs was injected at stock concentrations (1 μM) into fertilized zebrafish eggs at the one- or two-cell stage, and muscle recordings were performed at 72–86 hpf.

Online supplemental material

Fig. S1 shows the loss of inward rectification of single-channel currents for the αβδ receptor when recording in the outside-out patch configuration. Fig. S2 shows the effect of additional γ-subunit morpholinos and the γ/ε-subunit double-morpholino injections on the synaptic current kinetics and amplitude of both fast and slow muscle types. Figs. S1 and S2 are available at http://www.jgp.org/cgi/content/full/jgp.201110649/DC1.

RESULTS

Synaptic currents in fast and slow skeletal muscle

Whole cell voltage-clamp recordings of neuromuscular synaptic currents were obtained from both fast and slow twitch skeletal muscle at −90 mV. Consistent with previously published findings (Buss and Drapeau, 2000; Luna and Brehm, 2006), the decay time of slow muscle synaptic currents was greatly prolonged when compared with fast muscle counterparts (Fig. 1 A). Individual fast muscle synaptic currents decayed along a single-exponential time course (Fig. 1 A, left), with a mean 10–90% decay time constant (τ_{decay}) of 0.58 ± 0.1 ms (n = 894 events, 14 cells). Most slow muscle currents recorded were well fit by a single exponential with a mean τ_{decay} of 3.0 ± 0.7 ms (Fig. 1 A, right; n = 376 events, 15 cells). 17% of slow muscle synaptic currents required biexponential fits with mean τ_{decay} and associated weights corresponding to 0.43 ± 0.05 ms (20 ± 6%) and 3.5 ± 0.3 ms (80 ± 6%). For simplicity, only single-exponential decay events are considered in Fig. 1. Overall, there is an approximate fivefold slower decay for slow muscle as compared with fast muscle.

A potential mechanism for the prolonged current decays in zebrafish slow muscle is incomplete hydrolysis of ACh and resultant reopening of receptors (Drapeau et al., 2001). Precedent for this idea derives from developing *Xenopus* muscle where insufficient levels of acetylcholinesterase result in slowly rising and decaying synaptic current (Kullberg et al., 1977, 1980). To test for incomplete ACh hydrolysis in slow muscle, we recorded from a mutant line (*zim*^{tm205}) lacking functional acetylcholinesterase (Downes and Granato, 2004). Recordings revealed prolonged synaptic currents in both muscle types compared with wild-type fish (Fig. 1 B). The fast muscle currents were prolonged by ∼1.7-fold, and the decay was fit by single-exponential curves that averaged 1.0 ± 0.3 ms (−90 mV; n = 1,608 events, 28 cells). The slow muscle currents were prolonged by 1.2-fold, and decays were fit by single exponentials that averaged 3.7 ± 0.6 ms (−90 mV; n = 440 events, 15 cells). All events were included in a frequency histogram to compare distribution of decay times (Fig. 1 C). Synaptic decay distributions for each condition were individually fit to Gaussian functions, and the mean of each fit agreed well with the numerical average. The distribution of τ_{decay} for *zim*^{tm205} fast muscle remained essentially

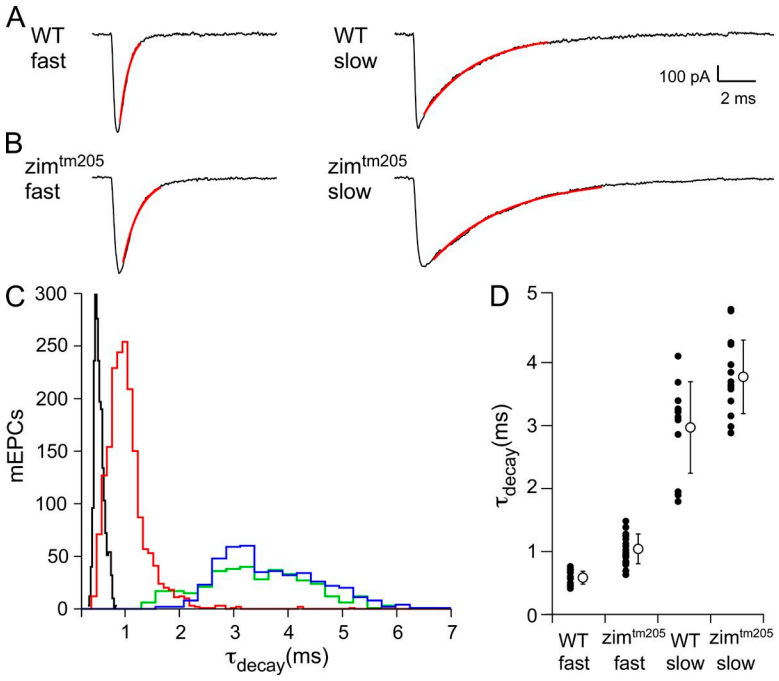

Figure 1. Comparison of decay time constants (τ_{decay}) of spontaneous synaptic currents (mEPCs) between wild-type and acetylcholinesterase-null (*zim*^{tm205}) 72–82-hpf larval zebrafish. (A) Sample mEPCs from wild-type fast (left) and wild-type slow (right) skeletal muscle. The 10–90% decay phase is fit to a single-exponential function (red) to obtain τ_{decay}. (B) Sample mEPCs from *zim*^{tm205} fast (left) and *zim*^{tm205} slow (right) skeletal muscle, each fit in the same manner as those in A. (C) The frequency histogram of τ_{decay} values for individual mEPCs from wild-type fast muscle (black; n = 14 recordings), *zim*^{tm205} fast muscle (red; n = 28 recordings), wild-type slow muscle (green; n = 15 recordings), and *zim*^{tm205} slow muscle (blue; n = 15 recordings). (D) The mean τ_{decay} values for each recording (filled circles) along with the overall mean ± SD (open circle) are shown for each condition.

nonoverlapping with slow muscle distribution (Fig. 1 C, compare red and green peaks). Furthermore, the average τ_{decay} plotted by individual cells also agreed well with the mean of the overall distribution (Fig. 1 D). For clarity, decay times were presented as cell averages for the remaining analyses. Because fast muscle currents in the acetylcholinesterase-null fish failed to mimic wild-type slow muscle synaptic current decay, the fivefold difference in synaptic kinetics cannot be accounted for by differences in ACh hydrolysis. Thus, we turned to cell-attached single-channel recordings to determine whether the differences reside in AChR channel-gating properties.

Single-channel ACh-activated currents in fast and slow skeletal muscle

On-cell recordings from fast skeletal muscle revealed two amplitude classes of ACh-activated single-channel currents (Fig. 2 A). The larger amplitude class was present in all 12 recordings, whereas the smaller amplitude class was observed in only 7 of 12 patches. In these patches, the smaller amplitude class accounted for 7 ± 3% of total openings. The mean amplitude for each class, determined by Gaussian fit of the amplitude frequency distribution, corresponded to −8.8 ± 0.6 pA and −6.6 ± 0.4 pA at +50 mV applied potential (Fig. 2 B). The current–voltage relationship for both the primary and secondary amplitude classes was linear between +100 and −30 mV applied potentials and corresponded to 68 ± 3.5 pS and 51 ± 3 pS, respectively (Fig. 2 C). The mean conductance ratio for the two classes was 1.34 ± 0.05 and matched the reported values for the expressed ε/γ AChR isoforms identified in mammalian and frog skeletal muscle (Hamill and Sakmann, 1981; Brehm et al., 1984; Mishina et al., 1986; Sullivan et al., 1999).

The mean burst open time for each conductance class was determined by exponential fit of the open-duration histograms (Fig. 2 D). Burst-duration histograms for the primary amplitude class of events were generally well fit to a single-exponential function with a mean time constant of 0.53 ± 0.06 ms at +50 mV applied potential (n = 10 patches; Fig. 2 D). The mean open burst duration for this class showed pronounced voltage dependence, decreasing when negative pipette voltages were used to depolarize the membrane patch. Fitting the burst duration versus applied potential relationship with an exponential function yielded an average e-fold change per 122 mV (Fig. 2 E; n = 8 recordings). Moreover, the mean values for single-channel burst duration associated with the primary amplitude class showed good agreement with the time constant for synaptic current decay in fast muscle (Fig. 3; 0.53 ± 0.06 vs. 0.58 ± 0.1; P = 0.2).

Because of the small number of openings, the mean values for burst duration for the secondary amplitude class varied considerably between patches. Consequently, the mean burst duration was determined on the basis of the arithmetic average value for each patch. At +50 mV applied potential, the burst duration ranged from 0.4 to 2.5 ms with a mean of 1.2 ± 0.8 ms (Fig. 2 D). This burst-duration value was longer than the time constant of synaptic decay in fast muscle (Fig. 3; P < 0.001). The absence of a slightly longer corresponding component of synaptic current decay was likely because of the small contribution to overall openings by this conductance class.

Single-channel recordings from slow muscle revealed ACh-activated events that were considerably longer in open duration than those of fast muscle (Fig. 4 A).

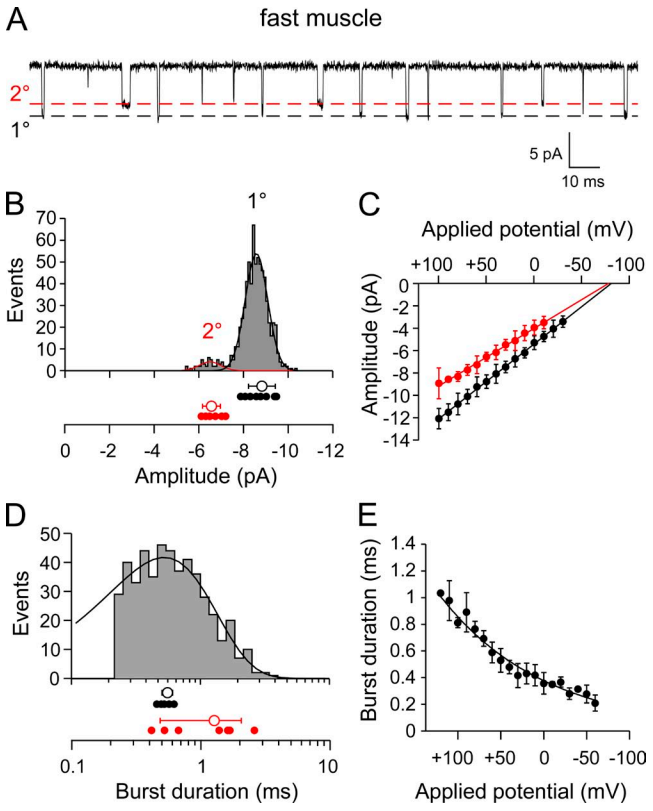

Figure 2. Single-channel ACh-activated currents from fast skeletal muscle of 72-hpf larval zebrafish. (A) A sample ~0.25-s trace showing two amplitude classes of ACh-activated channels (300 nM) recorded from a cell-attached patch at +30 mV applied potential. The open channel levels for the primary (1°) and secondary (2°) amplitude classes are indicated by the dashed lines. (B) The amplitude frequency histogram for openings recorded from a single patch at +50 mV applied potential. The mean value for each recording (filled symbols) is shown below the sample histogram for both the 1° and 2° classes, along with overall mean values ± SD (open circles). (C) The current–voltage relations for the 1° (black) and 2° (red) single-channel amplitude classes. Each symbol represents the mean amplitude ± SD values of all patches (n = 12) for each applied potential. (D) A burst-duration frequency histogram for the 1° amplitude class from a single recording fit with an exponential function. The mean burst-duration values for each recording of the 1° class (black filled symbols) and 2° class (red filled symbols) are shown along with the overall mean ± SD (open circles) below the histogram. (E) The relationship between applied potential and mean burst duration of the 1° amplitude class is exponential and corresponds to an e-fold change per 122 mV. Each symbol represents the mean ± SD (n = 8 recordings).

In 5 of 11 recordings at +50 mV applied potential, a single amplitude class was observed. In the balance of recordings a larger amplitude secondary class, comprising 12 ± 9% of total events, appeared as a right shoulder in the overall distribution (Fig. 4 B). The current–voltage relationship of the primary class of events was linear over applied potentials between +110 and −20 mV and resulted in an average conductance of 66 ± 2 pS (Fig. 4 C; $n = 8$). The secondary class conductance corresponded to 70 ± 4 pS.

The open burst-duration histogram for the primary event class in slow muscle required two exponential components for fit (Fig. 4 D). At +50 mV applied potential, the time constants were 3.5 ± 0.9 ms (41 ± 19%) and 0.23 ± 0.2 ms ($n = 10$ patches). Unlike fast muscle, the principal class in slow muscle showed a very weak dependence of burst duration on membrane potential (Fig. 4 E). The relations between mean burst duration and voltage, measured between +120 and +10 mV, were fit equally well by a linear and exponential curve. However, fitted to an exponential, the open burst duration exhibited an e-fold change per 263 mV ($n = 10$ patches). The secondary amplitude class was well fit by a single-exponential function with a time constant of 0.43 ± 0.1 ms (Fig. 4 D; $n = 4$ patches). This secondary class exhibited functional properties indistinguishable from the primary class present on fast muscle. Moreover, good agreement was found between the mean burst duration for the principal event class on slow muscle and the time constant of synaptic current decay (Fig. 3; 3.5 ± 0.9 ms vs. 3.0 ± 0.7; P = 0.26). Neither amplitude class on fast muscle bore the open burst-duration characteristics that corresponded to slow muscle synaptic current decay (Fig. 3).

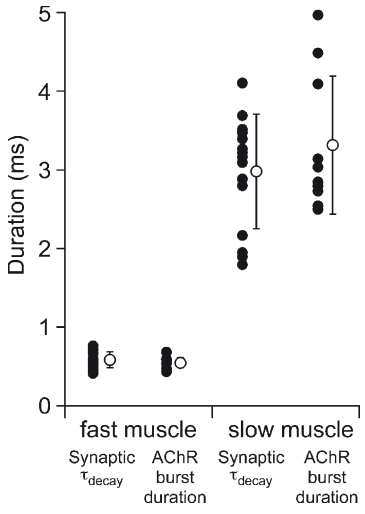

Figure 3. Comparison of single-channel mean burst duration and τ_{decay} of synaptic current for fast and slow muscle recordings. The mean values for individual recordings are indicated by filled symbols, and the overall mean ± SD is indicated as the open symbol for each condition.

Cloning and expression of zebrafish AChR subunits

We isolated cDNA encoding zebrafish AChR subunits for heterologous expression. Full-length sequences for α1 and δ, and partial sequences for β1, γ, and ε, were reported previously (Sepich et al., 1998; Ono et al., 2004; Etard et al., 2005). In Etard et al. (2005), only one β1-subunit cDNA was reported and analyzed. However, in puffer fish *Fugu rubripes*, two genes that are homologous

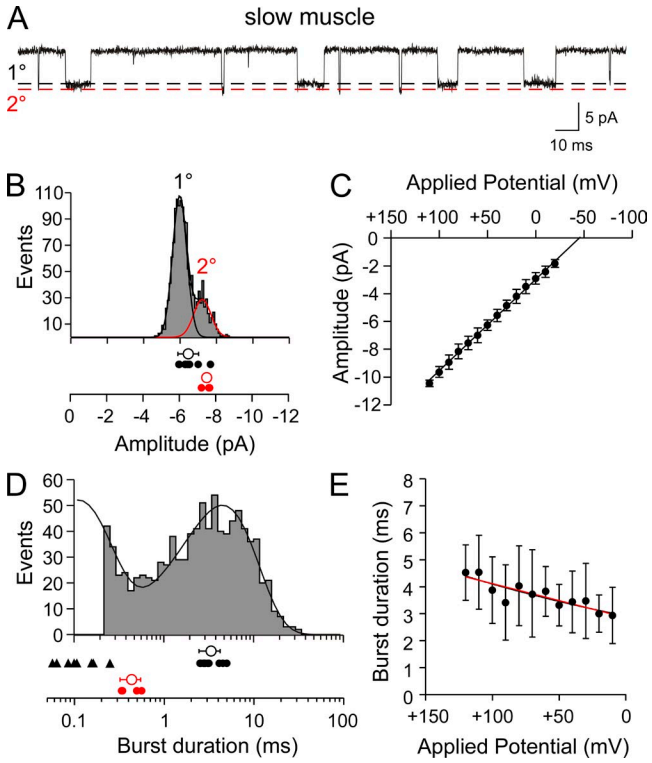

Figure 4. Single-channel ACh-activated currents from slow skeletal muscle of 72-hpf larval zebrafish. (A) A sample ~0.25-s trace showing two amplitude classes of ACh-activated channels (300 nM) recorded from a cell-attached patch at +50 mV applied potential. The open channel levels for the primary (1°) and secondary (2°) amplitude classes are indicated by the dashed lines. (B) The amplitude frequency histogram for a single recording with two amplitude classes (1° and 2°) at +50 mV applied potential. The mean values for each class are indicated for individual recordings (filled symbols) along the overall mean ± SD (open symbols) below the histogram. (C) The current–voltage relations for the pooled 1° openings. Each symbol represents the mean amplitude ± SD values of all patches ($n = 8$) for each applied potential. (D) A burst-duration frequency histogram from a single recording fit to the sum of two exponential functions. Only the 1° amplitude class was included in the distribution. The mean values for the brief (filled triangles) and long (filled circles) mean burst duration for the 1° class are indicated along with the overall mean ± SD (open symbols). The 2° class was fit separately to a single exponential (not depicted), and the individual mean values for burst duration for each recording (red filled circles) are indicated along with the overall mean ± SD (red open symbol). (E) The relationship between applied potential and mean burst duration is shown for all 1° class openings fit with linear (black) and exponential (red) curves. Each symbol represents the mean ± SD ($n = 10$ recordings).

to mammalian β1 were reported, named β1a and β1b (Jones et al., 2003). The clone reported in Etard et al. (2005) corresponded to β1b. We also identified a zebrafish cDNA homologous to β1a. Thus, full-length cDNAs encoding α1, β1a, β1b, γ, δ, and ε subunits were generated by PCR from zebrafish cDNA using specific primers and were used as templates for RNA synthesis (Fig. 5 A).

Functional expression for all candidate subunit combinations was first quantitated in *Xenopus* oocytes using two-electrode voltage clamp. The α-subunit RNA was included in all combinations tested, as the receptor could not function without the ACh-binding subunit. The α-subunit RNA was injected along with RNA for additional subunits and allowed 2–5 d to express functional receptors. Macroscopic responses were tested by applying 30 μM ACh (Fig. 5 B), which corresponded to a saturating concentration for receptors composed from the *Xenopus* subunits. As previously determined for *Torpedo*, the β-subunit RNA was also required for functional expression (Kurosaki et al., 1987). This was reflected in the absence of function corresponding to αδε-subunit expression (Fig. 5 C). The currents associated with any combination that included β1a RNA were so small that they precluded single-channel analyses. We used β1b for functional expression studies and will henceforth call this clone β for simplicity. Similarly, α1 is referred to as α. Of all RNA combinations tested, only αβδγ, αβδε, and αβδ expressed to very high levels sufficient for single-channel recording (Fig. 5 C).

Single-channel recordings were performed on outside-out patches derived from *Xenopus* oocytes. Although skeletal muscle was refractory to this recording configuration, outside-out patches formed readily from oocytes. Such patches provided low noise recordings of single-channel currents and manipulation of both external and cytoplasmic-facing solutions. For this purpose, patches were pulled from the animal side of the oocyte and exposed to 300 nM ACh. The first combination tested at the single-channel level was αβδε. Inspection of the openings indicated that they were very brief, and many events could not be fully resolved (Fig. 6 A). The majority of events recorded at −100 mV fell into a single major amplitude class (Fig. 6 B; $n = 12$ patches), although there were occasional smaller amplitude events that were not included in the analysis. The mean amplitudes at each potential were determined by Gaussian fit of the amplitude frequency histograms. The mean values, measured between −130 and −30 mV, were used to construct the current–voltage relations (Fig. 6 C). The average slope conductance was 66 ± 2 pS ($n = 8$ patches), which agrees with the primary class on fast muscle (Fig. 7 A; P = 0.23). Fitting the burst-duration histograms with a single-exponential function yielded an overall mean of 0.32 ± 0.05 ms at −100 mV ($n = 7$ patches). In most cases, however, the αβδε histograms were better described by a double-exponential function and yielded two mean burst durations of 0.54 ± 0.2 ms and 0.16 ± 0.06 ms (Fig. 6 D). For comparison with the burst-duration analysis of native muscle channels, the single-exponential fit values were used to determine

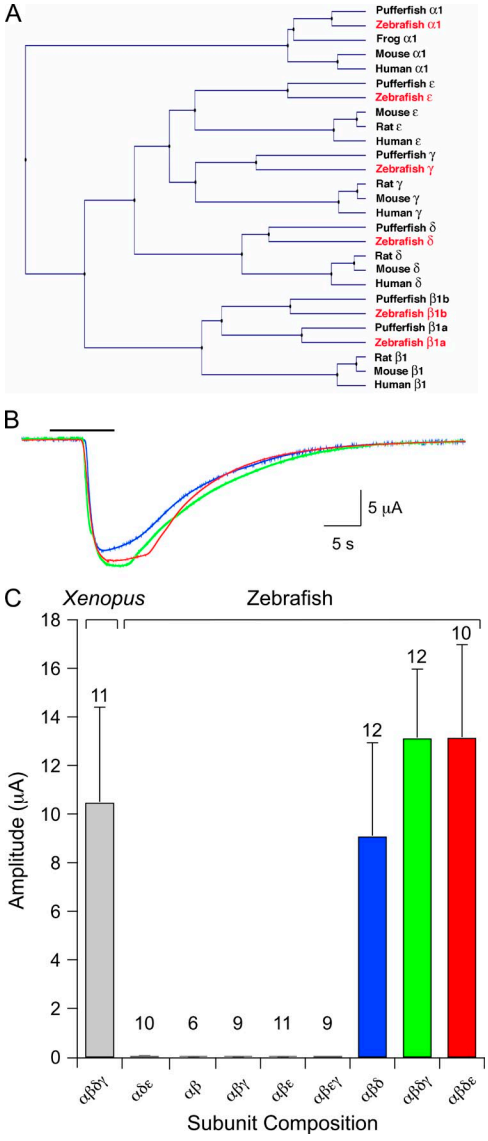

Figure 5. Zebrafish AChR subunit identification and functional expression in *Xenopus* oocytes. (A) A phylogenetic tree of AChR subunit genes constructed by the UPGMA method. Subunit sequences of human (*Homo sapiens*), mouse (*Mus musculus*), rat (*Rattus norvegicus*), puffer fish (*Takifugu rubripes*), and frog (*Xenopus tropicalis*) are included. Zebrafish genes are highlighted in red. (B) Two microelectrode recordings of membrane currents elicited by 30 μM ACh (bar) at a −80 mV holding potential. Shown are responses from oocytes expressing αβδε (red trace), αβδγ (green trace), or αβδ (blue trace) RNA. (C) The mean ± SD macroscopic current amplitude associated with the RNA subunit combinations is indicated. *Xenopus* αβδγ RNA is shown for comparison, and the number of oocytes tested is indicated for each RNA combination tested. The three combinations that yielded currents suitable for single-channel recordings are indicated by colored bars.

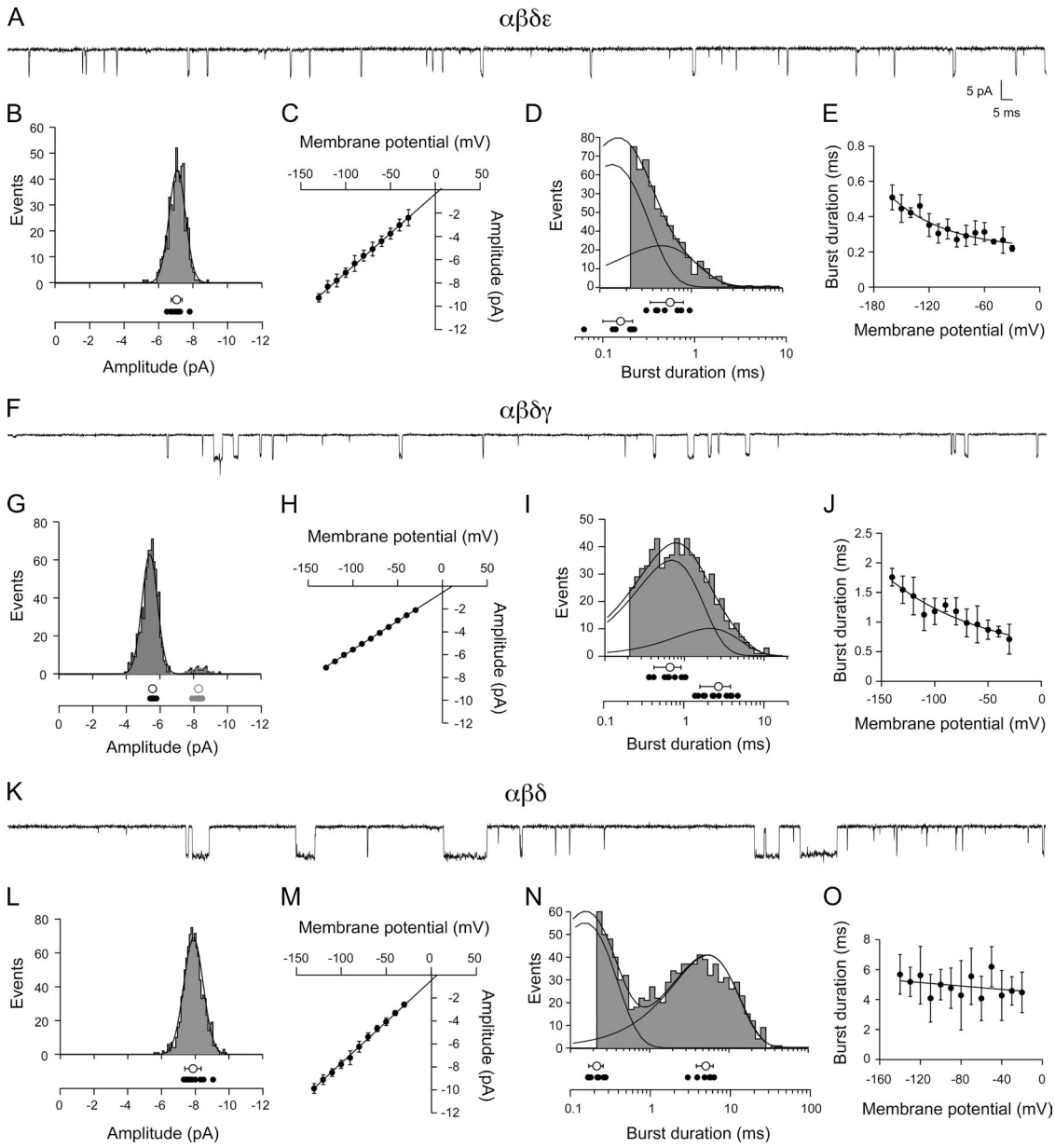

Figure 6. Functional properties of ACh-activated single-channel currents from *Xenopus* oocytes expressing αβδε (A–E), αβδγ (F–J), and αβδ (K–O) subunit RNA. (A) Sample recording from a patch expressing αβδε at −100 mV. (B) A representative amplitude histogram for one recording, with individual mean values for all recordings (filled circles; $n = 12$) shown below along with the overall mean ± SD (open circle) at −100 mV. (C) The cumulative current–voltage relations for eight recordings. (D) A representative burst-duration histogram fit by the sum of two exponentials. The time constants for each exponential are indicated for each recording (filled circles; $n = 7$) along with the overall mean ± SD for all recordings (open circles) at −100 mV. (E) The relationship between burst duration and membrane potential for seven recordings fit to an exponential function. The voltage dependence corresponds to e-fold change per 156 mV over this range. (F) Sample recording from a patch expressing αβδγ at −100 mV. (G) A representative amplitude histogram from one recording showing a 1° (black) and 2° (red) amplitude class of openings. The individual mean values for 10 recordings (filled circles) are shown along with the overall mean ± SD (open circles) for each class at −100 mV. (H) The cumulative current–voltage relations for the primary class for eight recordings. (I) A representative burst-duration histogram fit by the sum of two exponentials. The time constants for each exponential are indicated for each recording (filled circles; $n = 9$) as well as the overall mean ± SD (open circles) at −100 mV. (J) The relationship between burst duration and membrane potential for four recordings fit to an exponential function. The voltage dependence corresponds to e-fold change per 141 mV over this range. (K) Sample recording from a patch expressing αβδ at −100 mV. (L) A representative amplitude frequency histogram from a single recording with the individual mean values for all recordings (filled circles; $n = 13$) along with the overall mean ± SD (open circle) at −100 mV. (M) The cumulative current–voltage relations for 11 recordings. (N) A representative burst-duration histogram fit by the sum of two exponentials. The individual time constants for each exponential are indicated for each recording (filled circles; $n = 6$) as well as the overall mean ± SD for all recordings (open circles) at −100 mV. (O) The relationship between burst duration and membrane potential for six recordings fit to an exponential function over the range of values shown yielding an e-fold change in burst duration per 769 mV.

the voltage dependence of the burst duration and yielded an e-fold change per 156 mV (Fig. 6 E; $n = 7$ patches). Additionally, the burst-duration values of αβδε at −100 mV were not different from the burst duration of fast muscle receptors at comparable membrane potentials, as estimated by adjusting applied potential for resting membrane potentials (Fig. 7 B; P = 0.9).

Next, outside-out patches expressing αβδγ-subunit RNAs were tested. Quite unexpectedly, inspection of these openings revealed brief duration events that were visually similar to the αβδε-subunit combination (Fig. 6 F). The majority of events fell into a single amplitude class, but infrequent openings by a slightly larger amplitude channel class were observed in 8 of 10 patches (Fig. 6 G; $n = 8$ patches). The current–voltage relationship for the primary class averaged 51 ± 2 pS (Fig. 6 H; $n = 8$ patches) and was similar to the secondary amplitude class on fast muscle (Fig. 7 A; P = 0.3). When fit with a single exponential, the mean burst duration was 1.3 ± 0.4 ms ($n = 9$ patches). However, the burst histograms generated at −100 mV required two exponential components for adequate fitting (Fig. 6 I). The primary component of the open-duration histogram contributed 75 ± 11% of total events and corresponded to a time constant of 0.67 ± 0.3 ms, whereas the secondary component contributed 25 ± 11% and corresponded to a time constant of 2.7 ± 1.1 ms. The voltage dependence of the burst duration (determined by single-exponential burst-duration values) was fit by an exponential function yielding an e-fold change per 141 mV (Fig. 6 J; $n = 4$ patches). The conductance and burst duration (when comparing fits with single-exponential average) indicated that αβδγ receptor properties were not significantly different from the smaller amplitude openings seen occasionally in recordings from fast muscle (Fig. 7, A and B; P = 0.3 and P = 0.8).

The third subunit combination to express at levels adequate for single-channel recordings was αβδ (Fig. 6). Openings by αβδ receptors were conspicuously longer in duration than either αβδε and αβδγ counterparts (Fig. 6 K). The αβδ channels comprised a single amplitude class (Fig. 6 L; $n = 13$ patches) with a slope conductance of 70 ± 5 pS (Fig. 6 M; $n = 11$ patches). At 300 nM ACh, αβδ openings consistently required two exponential components to fit the burst histograms (Fig. 6 N; $n = 6$ patches). The slow component corresponded to 4.7 ± 1.2 ms and averaged 52 ± 17% of the total openings. The brief component was nearly equal in contribution (48 ± 17%) and corresponded to 0.22 ± 0.04 ms. The contribution by the fast component was essentially eliminated at high ACh concentration (10 μM), indicating that it might not represent openings by di-liganded receptors (unpublished data). The αβδ receptor relationship between burst duration and voltage was equally well described by an exponential or linear function between −20 and −140 mV (Fig. 6 O; $n = 6$); when fit with an exponential, the e-fold change in burst duration coincided with 769 mV. This property was similar to that observed for the receptors present on slow muscle (Fig. 4 E). Additionally, the αβδ and slow muscle receptors were similar in conductance (Fig. 7 A; P = 0.05) and in burst duration (Fig. 7 B; P = 0.08). By comparison, the burst duration of slow muscle receptors was highly dissimilar to that of both αβδε (Fig. 7 B; P < 0.0001) and αβδγ (P < 0.0001) channels.

Inward rectification of αβδ channels and slow muscle currents

Further comparison between slow muscle AChRs and heterologously expressed αβδ receptors was provided by the voltage dependence of single-channel conductance. It was possible to reverse the polarity of fast muscle on-cell single-channel ACh-activated currents with depolarizations positive to the reversal potential (Fig. 8 A). However, slow muscle patches that showed frequent openings

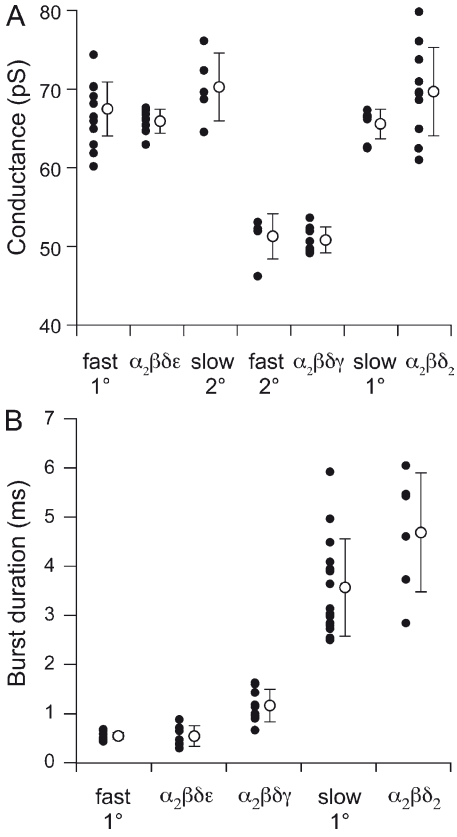

Figure 7. Comparisons between fast and slow muscle ACh-activated channels and individually identified receptor isoforms expressed in *Xenopus* oocytes. (A) Comparisons of single-channel conductance for $\alpha_2\beta\delta\varepsilon$, $\alpha_2\beta\delta\gamma$, and $\alpha_2\beta\delta_2$ receptor isoforms in oocytes to both the 1° and 2° amplitude classes from muscle. The values from individual recordings (filled circles) and overall mean ± SD values (open circles) are indicated for each condition. (B) Comparisons of single-channel mean burst duration of $\alpha_2\beta\delta\varepsilon$, $\alpha_2\beta\delta\gamma$, and $\alpha_2\beta\delta_2$ receptor isoforms to the mean burst duration of 1° fast and slow muscle receptors. The values from individual recordings are indicated by filled circles, and the overall mean ± SD values are indicated by the open circle for each condition.

at negative potentials did not exhibit openings at applied potentials corresponding to positive membrane potentials (Fig. 8 B). Restoring the potential to negative values immediately resulted in the resumption of inward going events, and this behavior stood in sharp contrast to the ability of fast muscle single-channel currents to reverse polarity at positive potentials. The current–voltage relations for fast muscle single-channel currents were linear for both inwardly and outwardly directed currents (not depicted).

Similarly, whole cell recordings of synaptic currents for slow muscle showed evidence of inward rectification. The mean amplitude of spontaneously occurring synaptic currents was measured over a range of potentials positive and negative to zero mV, corresponding to the receptor reversal potential. In fast muscle, the current-voltage relationship was linear over the range of 230 mV (Fig. 8 C), agreeing with previously published data (Wen and Brehm, 2005). However, in slow muscle the outwardly directed synaptic currents were smaller than the inward counterparts at equivalent potentials (Fig. 8 D).

To determine whether the αβδ-subunit combination also represented an inwardly rectifying muscle AChR, on-cell single-channel recordings were performed on *Xenopus* oocytes expressing αβδ subunits under identical conditions to those used for zebrafish muscle. On-cell single-channel openings from αβδ receptors failed to reverse sign at positive membrane potentials (Fig. 9 A). In contrast, on-cell single-channel openings from oocytes expressing αβδε subunits occurred at each potential tested, including positive membrane potentials (Fig. 9 B). Furthermore, two-electrode voltage-clamp measurements of macroscopic currents from αβδ-expressing oocytes also revealed pronounced inward rectification (Fig. 9 B). The current–voltage relations for macroscopic ACh-activated currents were obtained using a 2-s voltage ramp between −80 and +80 mV before (leak

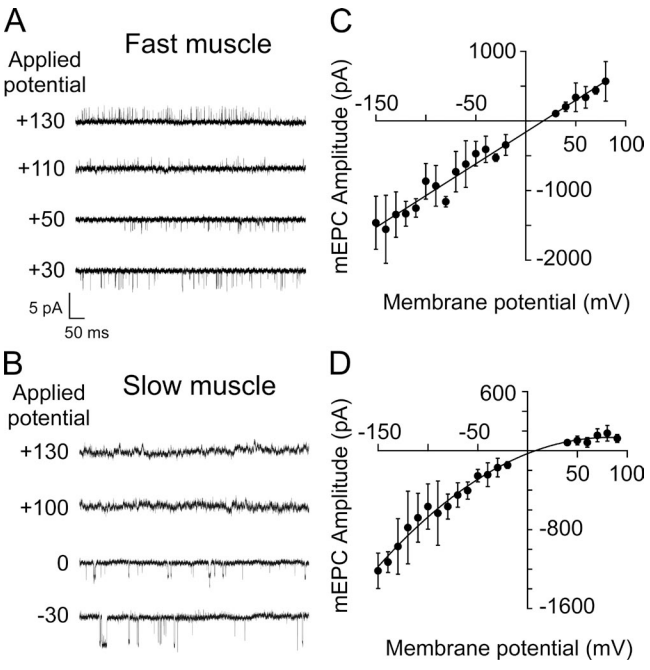

Figure 8. Differences in rectification between fast and slow muscle ACh-activated single-channel currents. Sample single-channel traces at holding potentials that are either positive or negative to the current reversal potential (∼0 mV) for fast muscle (A) and slow muscle (B). (C) The current–voltage relations for fast muscle synaptic currents, with each point representing the mean ± SD of seven recordings, fit by a linear curve. (D) The current–voltage relations for synaptic currents in slow muscle, with each point representing the mean ± SD for 10 recordings, fit by a second-order polynomial curve.

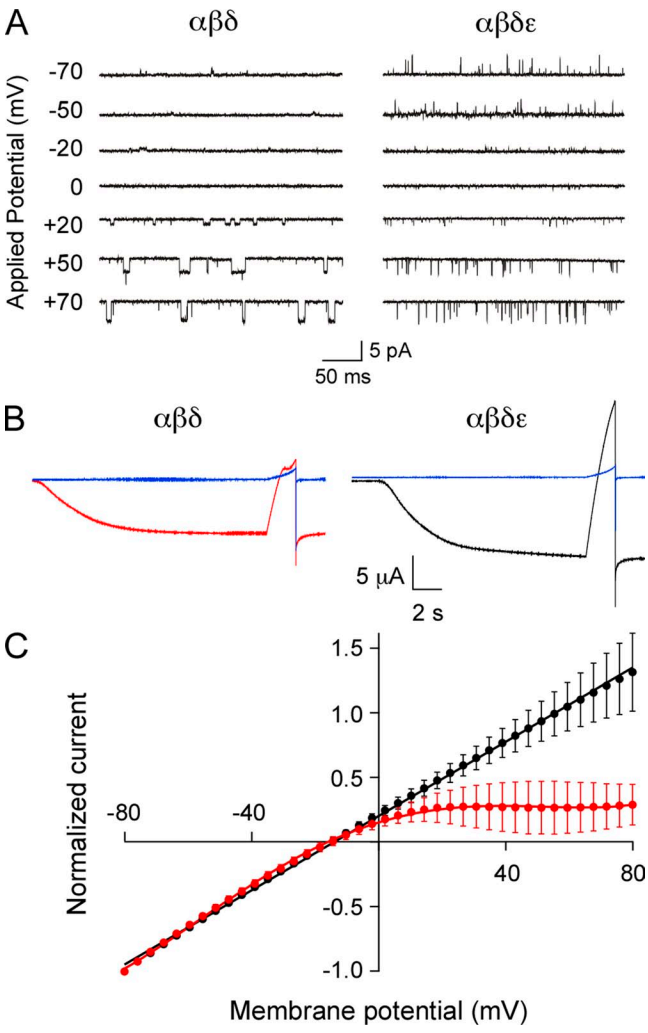

Figure 9. Inward rectification of the zebrafish αβδ channel isoform. (A) Sample ACh-activated single-channel currents recorded at the indicated potentials from cell-attached patches of *Xenopus* oocytes injected with either αβδ (left) or αβδε (right) RNA. (B) Whole oocyte ACh-activated macroscopic currents recorded at −80 mV and subsequently ramped from −80 to +80 mV over a 2-s period. Oocytes were either injected with αβδ (red) or αβδε (black). Leak currents recorded before ACh application are indicated in blue. (C) Current–voltage relations of macroscopic currents from αβδ (red; $n = 5$) and αβδε (black; $n = 3$) RNA-injected oocytes were normalized to peak current and fit with fifth-order polynomial (red) or linear curves (black).

current) and during application of 30 µM ACh (Fig. 9 B). However, even without leak current subtraction, the inward rectification of the macroscopic ACh current could be observed for αβδ (Fig. 9 B, left). In contrast, neither αβδε (Fig. 9 B, right) nor αβδγ currents (not depicted) showed evidence of inward rectification of macroscopic ACh-activated current. Averaged normalized current–voltage relations for αβδε (n = 3 oocytes) were well described by a linear fit between −80 and +80 mV, whereas $\alpha_2\beta\delta_2$ (n = 5 oocytes) required fitting with a fifth-order polynomial (Fig. 9 C). The inward rectification was abolished in αβδ-expressing oocytes only after formation of outside-out patches (Fig. S1), suggesting that inward rectification of αβδ channels may result from an extrinsic block mechanism similar to that seen for other receptor types, including neuronal nicotinic receptors (Haghighi and Cooper, 1998).

Functional consequences of AChR subunit knockdown in vivo

The distinction between AChR isoforms in conferring fast versus slow muscle synaptic kinetics was further tested by knocking down the levels of individual subunit expression in vivo using morpholino antisense oligonucleotides. Each subunit-specific morpholino was injected into newly fertilized wild-type eggs at the single-cell stage, and recordings of synaptic current were performed at 72–96 hpf. The effectiveness of this approach was first tested in fast muscle by measuring spontaneous synaptic current amplitudes in response to injection of a morpholino designed to block translation of the α-subunit transcript. Mean synaptic current amplitudes measured at −70 mV in fast muscle cells were significantly reduced in fish treated with α-subunit morpholino (−146 ± 95 pA) as compared with wild-type fish (−757 ± 284 pA; Fig. 10 A; $P < 0.001$). Similarly, the mean synaptic current amplitude in slow muscle was also reduced with α morpholino (−258 ± 97 pA) compared with wild-type fish (−413 ± 103 pA; Fig. 10 B; $P < 0.01$). However, the synaptic current kinetics measured at −70 mV in both fast (Fig. 10 C) and slow muscle (Fig. 10 D) remained unchanged compared with wild type.

Next tested was a morpholino designed to block translation of the γ-subunit transcript. The mean amplitude and kinetics of synaptic responses remained unchanged in both muscle types (Fig. 10, A–D). To further investigate these findings, two additional morpholinos were tested: a second translation site blocking morpholino, and a morpholino designed to alter γ-transcript splicing. Similar results were obtained with the additional γ morpholinos, in that synaptic responses were also indistinguishable from wild type in amplitude and kinetics (Fig. S2). To confirm that our morpholinos reduced the γ-subunit protein levels, we monitored the γ transcript after treatment with the splice acceptor site morpholino to independently measure the morpholino efficacy. PCR and subsequent sequencing confirmed that the morpholino resulted in γ transcripts that were aberrantly processed in the manner predicted by the splice-blocking site, greatly reducing the presence of wild-type γ transcript (not depicted). Therefore, the inability of the γ morpholinos to alter fast and slow muscle synaptic kinetics likely reflects the minor role of this subunit in synaptic function at this stage of neuromuscular development.

The ε-subunit morpholino had a pronounced effect on fast muscle synaptic current, wherein the decay was greatly prolonged compared with wild type (Fig. 10 C). Most of the synaptic currents decayed along a biexponential time course, with time constants averaging 0.52 ± 0.2 and 2.3 ± 0.5 ms. The brief time constant was similar to that of synaptic currents in wild-type fast muscle (P = 0.06). Moreover, the long time constant was similar to

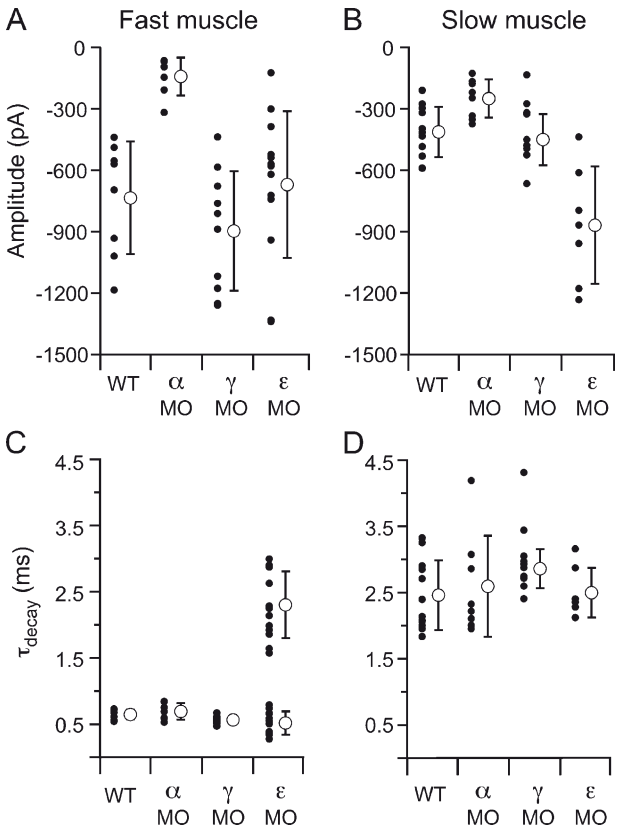

Figure 10. Comparison of synaptic current properties after α, γ, and ε AChR subunit knockdown in fast and slow muscle. All recordings were performed at a −70 mV holding potential. (A) Mean amplitude of spontaneous synaptic currents recorded from fast muscle for individual cells (filled circles) and overall mean ± SD (open circles) for each condition. (B) Mean amplitude of spontaneous synaptic currents recorded from slow muscle for individual cells (filled circles) and overall mean ± SD (open circles) for each condition. (C) Mean τ_{decay} values for individual fast muscle recordings (filled circles) and overall mean ± SD (open circles) for each condition. (D) Mean τ_{decay} values for individual slow muscle recordings (filled circles) and overall mean ± SD (open circles) for each condition.

the decay time constant associated with slow muscle synaptic currents (P = 0.5). The fast component comprised 37 ± 21% of the current amplitude, and the slow component comprised 62 ± 20%. Although an indirect measurement, the biexponential synaptic kinetics suggested that a mixed population of receptor types was present at the synapse (presumably $\alpha\beta\delta\varepsilon$ and $\alpha\beta\delta$), likely resulting from incomplete elimination of the ε-subunit protein. To examine the possibility that the remaining fast component of synaptic transmission in ε morpholino–treated fish could be a result of the presence of the γ subunit, synaptic responses were examined in fish coinjected with ε and one of the γ morpholinos. The synaptic responses were not different in ε/γ double-morphant fish compared with ε alone (Fig. S2). This finding is consistent with the idea that the residual fast component of the ε morpholino–treated fish reflects an incomplete knockdown of ε and not the expression of a receptor containing a γ subunit. Although the kinetics of fast muscle synaptic currents were prolonged in the ε-morpholino fish, the amplitude was not different than wild type (Fig. 10 A). The kinetics of slow muscle synaptic responses were not altered by the ε morpholino (Fig. 10 D), but a significant increase in amplitude was observed (Fig. 10 B; P = 0.005). The underlying basis for the change in amplitude is uncertain but may result from compensatory increases in $\alpha\beta\delta$ expression and the associated increase in open probability.

DISCUSSION

In skeletal muscle, the $\alpha\beta\delta\gamma$- and $\alpha\beta\delta\varepsilon$-subunit combinations result in the formation of nicotinic receptor isoforms with stoichiometries of $\alpha_2\beta\delta\gamma$ and $\alpha_2\beta\delta\varepsilon$, respectively. The $\alpha_2\beta\delta\gamma$ isoform mediates transmission in embryonic muscle, whereas the $\alpha_2\beta\delta\varepsilon$ isoform predominates in adult skeletal muscle. This assignment has been based on numerous molecular and physiological studies of both mammalian and *Xenopus* skeletal muscle (Mishina et al., 1986; Witzemann et al., 1987; Gu and Hall, 1988; Camacho et al., 1993; Missias et al., 1996). Thus, it came as no surprise when the genes coding for the ε and γ subunits were also identified in the puffer fish genome (Jones et al., 2003) and when single-channel recordings in zebrafish revealed two event classes bearing the signature amplitude ratios for ε- and γ-containing receptors (Nguyen et al., 1999). At embryonic synapses where receptor density is low, the $\alpha_2\beta\delta\gamma$ receptor isoform provides for effective depolarization by virtue of its long burst time (Jaramillo et al., 1988). In contrast, our findings indicate that the zebrafish $\alpha_2\beta\delta\gamma$ receptor has a burst duration that is only slightly longer than the $\alpha_2\beta\delta\varepsilon$ isoform, and furthermore, that the $\alpha_2\beta\delta\gamma$ receptor does not contribute to synaptic currents at 72 hpf. It is possible that $\alpha_2\beta\delta\gamma$ contributes to synaptic decay at development times even earlier than 72 hpf, the earliest time point we examined. We observed a steady decline of γ transcripts in whole fish over the first week of development, and γ-subunit transcripts could not be detected in adult zebrafish (unpublished data). The absence of a significant functional role at 72 hpf is also supported by the lack of effect of morpholino knockdown of γ subunit in fast and slow muscle types. In contrast, knockdown of ε subunit prolonged the synaptic current decay in fast muscle, presumably through mis-expression of ε/γ-less channels. Thus, control over synaptic current time course in fast muscle is attributed to the $\alpha_2\beta\delta\varepsilon$ receptor type, similar to all previous reports from fast vertebrate skeletal muscle (Mishina et al., 1986; Witzemann et al., 1987; Gu and Hall, 1988; Camacho et al., 1993; Missias et al., 1996).

Heterologously expressed $\alpha_2\beta\delta\varepsilon$ and $\alpha_2\beta\delta\gamma$ receptors did not match convincingly the functional properties of slow muscle single-channel currents. The burst duration for $\alpha_2\beta\delta\gamma$ was too brief, and the conductance was much too low. The $\alpha_2\beta\delta\varepsilon$ conductance was similar to slow muscle channels, but the mean burst duration was much too brief. An alternative proposal for the origin of slow muscle synaptic currents in zebrafish is incomplete hydrolysis of ACh (Drapeau et al., 2001). Slowed hydrolysis would be expected to result in repeated openings of receptors during transmission and prolongation of synaptic current. In developing *Xenopus* myotomal muscle, low levels of acetylcholinesterase were shown to contribute to the slow rise and decay of synaptic current (Kullberg et al., 1977, 1980). We tested this proposal for slow versus fast muscle in acetylcholinesterase-null zebrafish using the homozygous mutants produced by the strain *zim*^{tm205} (Downes and Granato, 2004). Zebrafish harbors a single gene encoding acetylcholinesterase (Bertrand et al., 2001), so it is likely that active transmitter hydrolysis is abolished at mutant neuromuscular synapses. At 72–96 hpf, both fast and slow muscle synaptic currents of *zim*^{tm205} fish were prolonged when compared with wild-type currents. However, the extent of prolongation in fast muscle was well short of matching the long decay of wild-type slow muscle synaptic current. This finding ruled out the possibility that differences in cholinesterase activity between fast and slow muscle synapses alone governed the kinetic differences.

Evidence for a nontraditional AChR isoform on slow muscle was provided through *Xenopus* oocyte expression of zebrafish AChR subunit RNAs. Several lines of evidence support the assertion that $\alpha_2\beta\delta_2$ represents the slow muscle receptor isoform. First, the mean burst duration of expressed $\alpha_2\beta\delta_2$ receptor channels matched both the burst duration of native slow muscle receptors and the time constants of synaptic current decay. Second, the uncharacteristically shallow voltage dependence of the burst duration was similar between the native slow muscle receptor and the expressed $\alpha_2\beta\delta_2$ receptor. This stands in sharp contrast to the voltage

dependence of burst duration observed for both $\alpha_2\beta\delta\gamma$ and $\alpha_2\beta\delta\varepsilon$ receptors. Third, knockdown of either ε- or γ-subunit expression failed to alter the kinetics of slow muscle synaptic currents, consistent with the idea that neither subunit is required for slow muscle AChR function. Finally, $\alpha_2\beta\delta_2$ macroscopic currents in oocytes show pronounced inward rectification, similar to the single-channel and synaptic currents recorded from slow muscle. This rectification property is lost upon formation of outside-out patches, pointing to the existence of an extrinsic modulator of voltage-dependent block (Haghighi and Cooper, 1998). Neither $\alpha_2\beta\delta\varepsilon$ nor $\alpha_2\beta\delta\gamma$ receptors showed pronounced inward rectification under any recording conditions.

The ability of γ/ε-less receptors to express functional currents in heterologous cells has been well documented. Specifically, expression of α-, β-, and δ-subunit RNA from *Torpedo* (Golino and Hamill, 1992), *Xenopus* (Paradiso and Brehm, 1998), mouse (Liu and Brehm, 1993), and bovine (Jackson et al., 1990) cDNAs all yielded robust ACh-activated currents in *Xenopus* oocytes. Biochemical analyses of receptors expressed in HEK cells indicated that the receptors formed as pentamers with a stoichiometry corresponding to $\alpha_2\beta\delta_2$ (Sine and Claudio, 1991). There are few studies that would shed light on a role of γ/ε-less receptors in muscle. However, the mouse γ-subunit knockout shows prominent movement and associated synaptic current at an age that precedes ε expression (Liu et al., 2010).

Recently, a muscle nicotinic receptor formed by only three different subunits was shown to mediate swimming contractions in the larval tunicate *Ciona* (Nishino et al., 2011). The receptor was thought to contain two α subunits along with three copies of a second type of subunit termed BGDE3, based on its shared homology to vertebrate β, γ, δ, and ε subunits. This receptor type exhibited inward rectification, setting it apart from all skeletal muscle type receptors described to date. The BGDE3 subunit contained a glutamate residue at the "intermediate ring" position (Fig. 11), a residue previously shown to be critical to channel rectification in the α subunit of the neuronal nicotinic receptor $\alpha_3\beta_4$ (Haghighi and Cooper, 2000). The muscle receptor subunits γ and ε contain uncharged glutamine residues at this position (Fig. 11), and receptors containing either subunit show linear current–voltage relations. As was shown for the neuronal receptor type, inward rectification of the *Ciona* muscle receptor was abolished when the glutamate at the intermediate ring position was replaced with glutamine. The zebrafish δ subunit contains the charged glutamate residue present in *Ciona*, rat neuronal receptors, and mammalian δ subunits (Fig. 11). Also, like their vertebrate counterparts, the zebrafish γ and ε subunits are uncharged at this position (Fig. 11). Consequently, the $\alpha_2\beta\delta_2$ receptor in zebrafish would be expected to exhibit greater charge in the intermediate ring, consistent with the strong rectification seen in single-channel and macroscopic currents.

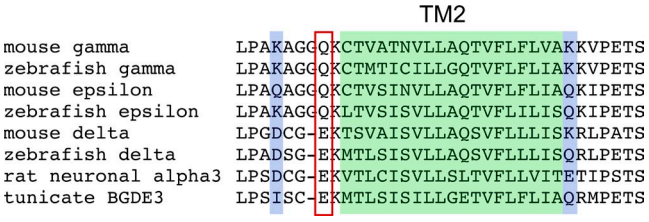

Figure 11. Alignment of residues within AChR subunits of different species. The residues outlined with red form the intermediate charged ring and have been shown to be involved in channel rectification of rat neuronal α3 and tunicate BDGE3 subunit–containing receptors. The second transmembrane region (TM2) is indicated by the shaded green, and the outer and inner charged rings are indicated by the blue shade.

It appears then, that the absence of γ and ε subunits in both tunicate and zebrafish slow muscle AChRs impart the functional properties that are more neuronal-like than traditional muscle receptors (Haghighi and Cooper, 2000). Additionally, studies on both *Ciona* and neuronal receptors revealed an increased permeability to calcium compared with traditional muscle receptors. In the case of *Ciona*, the entry of calcium through the muscle receptor was shown to be a direct mediator of the slow contractions (Nishino et al., 2011). As with *Ciona* muscle, the slow muscle of zebrafish fails to generate an action potential, suggesting that the receptors in both cases play a more direct role in mediating the contractility than they do in traditional excitable skeletal muscle. It remains to be determined whether the γ/ε-less receptor isoform represents a primitive receptor present only in early proto-chordates and chordates or alternatively serves a more widespread role in mediating neuromuscular transmission in the specialized muscle types of higher vertebrates.

We thank Chris Alexander and Dr. David Dawson for generously providing oocytes and Dr. Hua Wen for experimental advice.

Support was provided by National Institutes of Health (grant NS-18205 to P. Brehm) and Howard Hughes Medical Institute (G. Mandel).

Angus C. Nairn served as editor.

Submitted: 8 April 2011
Accepted: 1 August 2011

REFERENCES

Bertrand, C., A. Chatonnet, C. Takke, Y.L. Yan, J. Postlethwait, J.P. Toutant, and X. Cousin. 2001. Zebrafish acetylcholinesterase is encoded by a single gene localized on linkage group 7. Gene structure and polymorphism; molecular forms and expression pattern during development. *J. Biol. Chem.* 276:464–474. doi:10.1074/jbc.M006308200

Bondi, A.Y., D.J. Chiarandini, and J. Jacoby. 1986. Induction of action potentials by denervation of tonic fibres in rat extraocular muscles. *J. Physiol.* 374:165–178.

Brehm, P., Y. Kidokoro, and F. Moody-Corbett. 1984. Acetylcholine receptor channel properties during development of Xenopus muscle cells in culture. *J. Physiol.* 357:203–217.

Buckingham, S.D., and D.W. Ali. 2004. Sodium and potassium currents of larval zebrafish muscle fibres. *J. Exp. Biol.* 207:841–852. doi:10.1242/jeb.00839

Buss, R.R., and P. Drapeau. 2000. Physiological properties of zebrafish embryonic red and white muscle fibers during early development. *J. Neurophysiol.* 84:1545–1557.

Camacho, P., Y. Liu, G. Mandel, and P. Brehm. 1993. The ε subunit confers fast channel gating on multiple classes of acetylcholine receptors. *J. Neurosci.* 13:605–613.

Charnet, P., C. Labarca, and H.A. Lester. 1992. Structure of the γ-less nicotinic acetylcholine receptor: learning from omission. *Mol. Pharmacol.* 41:708–717.

Dionne, V.E. 1989. Two types of nicotinic acetylcholine receptor channels at slow fibre end-plates of the garter snake. *J. Physiol.* 409:313–331.

Dionne, V.E., and R.L. Parsons. 1978. Synaptic channel gating differences at snake twitch and slow neuromuscular junctions. *Nature.* 274:902–904. doi:10.1038/274902a0

Dionne, V.E., and R.L. Parsons. 1981. Characteristics of the acetylcholine-operated channel at twitch and slow fibre neuromuscular junctions of the garter snake. *J. Physiol.* 310:145–158.

Downes, G.B., and M. Granato. 2004. Acetylcholinesterase function is dispensable for sensory neurite growth but is critical for neuromuscular synapse stability. *Dev. Biol.* 270:232–245. doi:10.1016/j.ydbio.2004.02.027

Drapeau, P., R.R. Buss, D.W. Ali, P. Legendre, and R.L. Rotundo. 2001. Limits to the development of fast neuromuscular transmission in zebrafish. *J. Neurophysiol.* 86:2951–2956.

Etard, C., M. Behra, R. Ertzer, N. Fischer, S. Jesuthasan, P. Blader, R. Geisler, and U. Strähle. 2005. Mutation in the delta-subunit of the nAChR suppresses the muscle defects caused by lack of Dystrophin. *Dev. Dyn.* 234:1016–1025. doi:10.1002/dvdy.20592

Fedorov, V.V., L.G. Magazanik, V.A. Snetkov, and A.L. Zefirov. 1982. Postsynaptic currents in different types of frog muscle fibre. *Pflugers Arch.* 394:202–210. doi:10.1007/BF00589092

Fischbach, G.D., and S.M. Schuetze. 1980. A post-natal decrease in acetylcholine channel open time at rat end-plates. *J. Physiol.* 303:125–137.

Gilly, W.F., and C.S. Hui. 1980. Mechanical activation in slow and twitch skeletal muscle fibres of the frog. *J. Physiol.* 301:137–156.

Golino, M.D., and O.P. Hamill. 1992. Subunit requirements for *Torpedo* AChR channel expression: a specific role for the delta-subunit in voltage-dependent gating. *J. Membr. Biol.* 129:297–309.

Gu, Y., and Z.W. Hall. 1988. Immunological evidence for a change in subunits of the acetylcholine receptor in developing and denervated rat muscle. *Neuron.* 1:117–125. doi:10.1016/0896-6273(88)90195-X

Haghighi, A.P., and E. Cooper. 1998. Neuronal nicotinic acetylcholine receptors are blocked by intracellular spermine in a voltage-dependent manner. *J. Neurosci.* 18:4050–4062.

Haghighi, A.P., and E. Cooper. 2000. A molecular link between inward rectification and calcium permeability of neuronal nicotinic acetylcholine alpha3beta4 and alpha4beta2 receptors. *J. Neurosci.* 20:529–541.

Hamill, O.P., and B. Sakmann. 1981. Multiple conductance states of single acetylcholine receptor channels in embryonic muscle cells. *Nature.* 294:462–464. doi:10.1038/294462a0

Henderson, L.P., and P. Brehm. 1989. The single-channel basis for the slow kinetics of synaptic currents in vertebrate slow muscle fibers. *Neuron.* 2:1399–1405. doi:10.1016/0896-6273(89)90078-0

Hidaka, T., and N. Toida. 1969. Biophysical and mechanical properties of red and white muscle fibres in fish. *J. Physiol.* 201:49–59.

Jackson, M.B., K. Imoto, M. Mishina, T. Konno, S. Numa, and B. Sakmann. 1990. Spontaneous and agonist-induced openings of an acetylcholine receptor channel composed of bovine muscle alpha-, beta- and delta-subunits. *Pflugers Arch.* 417:129–135. doi:10.1007/BF00370689

Jaramillo, F., S. Vicini, and S.M. Schuetze. 1988. Embryonic acetylcholine receptors guarantee spontaneous contractions in rat developing muscle. *Nature.* 335:66–68. doi:10.1038/335066a0

Jones, A.K., G. Elgar, and D.B. Sattelle. 2003. The nicotinic acetylcholine receptor gene family of the pufferfish, Fugu rubripes. *Genomics.* 82:441–451. doi:10.1016/S0888-7543(03)00153-8

Kullberg, R.W., T.L. Lentz, and M.W. Cohen. 1977. Development of the myotomal neuromuscular junction in *Xenopus laevis*: an electrophysiological and fine-structural study. *Dev. Biol.* 60:101–129. doi:10.1016/0012-1606(77)90113-0

Kullberg, R.W., F.S. Mikelberg, and M.W. Cohen. 1980. Contribution of cholinesterase to developmental decreases in the time course of synaptic potentials at an amphibian neuromuscular junction. *Dev. Biol.* 75:255–267. doi:10.1016/0012-1606(80)90161-X

Kullberg, R.W., P. Brehm, and J.H. Steinbach. 1981. Nonjunctional acetylcholine receptor channel open time decreases during development of *Xenopus* muscle. *Nature.* 289:411–413. doi:10.1038/289411a0

Kurosaki, T., K. Fukuda, T. Konno, Y. Mori, K. Tanaka, M. Mishina, and S. Numa. 1987. Functional properties of nicotinic acetylcholine receptor subunits expressed in various combinations. *FEBS Lett.* 214:253–258. doi:10.1016/0014-5793(87)80065-0

Liu, Y., and P. Brehm. 1993. Expression of subunit-omitted mouse nicotinic acetylcholine receptors in *Xenopus laevis* oocytes. *J. Physiol.* 470:349–363.

Liu, Y., Y. Sugiura, D. Padgett, and W. Lin. 2010. Postsynaptic development of the neuromuscular junction in mice lacking the gamma-subunit of muscle nicotinic acetylcholine receptor. *J. Mol. Neurosci.* 40:21–26. doi:10.1007/s12031-009-9248-x

Luna, V.M., and P. Brehm. 2006. An electrically coupled network of skeletal muscle in zebrafish distributes synaptic current. *J. Gen. Physiol.* 128:89–102. doi:10.1085/jgp.200609501

Michler, A., and B. Sakmann. 1980. Receptor stability and channel conversion in the subsynaptic membrane of the developing mammalian neuromuscular junction. *Dev. Biol.* 80:1–17. doi:10.1016/0012-1606(80)90494-7

Miledi, R., and O.D. Uchitel. 1981. Properties of postsynaptic channels induced by acetylcholine in different frog muscle fibres. *Nature.* 291:162–165. doi:10.1038/291162a0

Mishina, M., T. Takai, K. Imoto, M. Noda, T. Takahashi, S. Numa, C. Methfessel, and B. Sakmann. 1986. Molecular distinction between fetal and adult forms of muscle acetylcholine receptor. *Nature.* 321:406–411. doi:10.1038/321406a0

Missias, A.C., G.C. Chu, B.J. Klocke, J.R. Sanes, and J.P. Merlie. 1996. Maturation of the acetylcholine receptor in skeletal muscle: regulation of the AChR γ-to-ε switch. *Dev. Biol.* 179:223–238. doi:10.1006/dbio.1996.0253

Nguyen, P.V., L. Aniksztejn, S. Catarsi, and P. Drapeau. 1999. Maturation of neuromuscular transmission during early development in zebrafish. *J. Neurophysiol.* 81:2852–2861.

Nishino, A., S.A. Baba, and Y. Okamura. 2011. A mechanism for graded motor control encoded in the channel properties of the muscle ACh receptor. *Proc. Natl. Acad. Sci. USA.* 108:2599–2604. doi:10.1073/pnas.1013547108

Ono, F., G. Mandel, and P. Brehm. 2004. Acetylcholine receptors direct rapsyn clusters to the neuromuscular synapse in zebrafish. *J. Neurosci.* 24:5475–5481. doi:10.1523/JNEUROSCI.0851-04.2004

Paradiso, K., and P. Brehm. 1998. Long-term desensitization of nicotinic acetylcholine receptors is regulated via protein kinase A-mediated phosphorylation. *J. Neurosci.* 18:9227–9237.

Ruff, R.L., and P. Spiegel. 1990. Ca sensitivity and acetylcholine receptor currents of twitch and tonic snake muscle fibers. *Am. J. Physiol.* 259:C911–C919.

Sakmann, B., and H.R. Brenner. 1978. Change in synaptic channel gating during neuromuscular development. *Nature.* 276:401–402. doi:10.1038/276401a0

Sepich, D.S., J. Wegner, S. O'Shea, and M. Westerfield. 1998. An altered intron inhibits synthesis of the acetylcholine receptor alpha-subunit in the paralyzed zebrafish mutant nic1. *Genetics.* 148:361–372.

Sigworth, F.J., and S.M. Sine. 1987. Data transformations for improved display and fitting of single-channel dwell time histograms. *Biophys. J.* 52:1047–1054. doi:10.1016/S0006-3495(87)83298-8

Sine, S.M., and T. Claudio. 1991. Gamma- and delta-subunits regulate the affinity and the cooperativity of ligand binding to the acetylcholine receptor. *J. Biol. Chem.* 266:19369–19377.

Stefani, E., and A.B. Steinbach. 1969. Resting potential and electrical properties of frog slow muscle fibres. Effect of different external solutions. *J. Physiol.* 203:383–401.

Sullivan, M.P., J.L. Owens, and R.W. Kullberg. 1999. Role of M2 domain residues in conductance and gating of acetylcholine receptors in developing *Xenopus* muscle. *J. Physiol.* 515:31–39. doi:10.1111/j.1469-7793.1999.031ad.x

Uchitel, O.D., and R. Miledi. 1987. Characteristics of synaptic currents in frog muscle fibers of different types. *J. Neurosci. Res.* 17:189–198. doi:10.1002/jnr.490170215

Wen, H., and P. Brehm. 2005. Paired motor neuron-muscle recordings in zebrafish test the receptor blockade model for shaping synaptic current. *J. Neurosci.* 25:8104–8111. doi:10.1523/JNEUROSCI.2611-05.2005

Wen, H., and P. Brehm. 2010. Paired patch clamp recordings from motor-neuron and target skeletal muscle in zebrafish. *J. Vis. Exp.* 2351.

Witzemann, V., B. Barg, Y. Nishikawa, B. Sakmann, and S. Numa. 1987. Differential regulation of muscle acetylcholine receptor γ- and ε-subunit mRNAs. *FEBS Lett.* 223:104–112. doi:10.1016/0014-5793(87)80518-5